NeuroImage: Clinical 26 (2020) 102234

Contents lists available at ScienceDirect

NeuroImage: Clinical

journal homepage: www.elsevier.com/locate/ynicl

Rotating frame MRI relaxations as markers of diffuse white matter abnormalities in multiple sclerosis

Pavel Filip[a,b], Alena Svatkova[c,d], Adam F Carpenter[e], Lynn E Eberly[b,f], Igor Nestrasil[c], Mikko J Nissi[g], Shalom Michaeli[b], Silvia Mangia[b,*]

[a] First Department of Neurology, Faculty of Medicine, Masaryk University and University Hospital of St. Anne, Brno, Czech Republic
[b] Department of Radiology, Center for Magnetic Resonance Research (CMRR), University of Minnesota, Minneapolis, MN, USA
[c] Department of Pediatrics, University of Minnesota, Minneapolis, MN, USA
[d] Department of Medicine III, Clinical Division of Endocrinology and Metabolism, Medical University of Vienna, Vienna, Austria
[e] Department of Neurology, School of Medicine, University of Minnesota, Minneapolis, MN, USA
[f] Division of Biostatistics, School of Public Health, University of Minnesota, Minneapolis, MN, USA
[g] Department of Applied Physics, University of Eastern Finland, Kuopio, Finland

ARTICLE INFO

Keywords:
Multiple sclerosis
Rotating frame relaxation MRI
Adiabatic pulses
DTI
T1w/T2w ratio

ABSTRACT

Even though MRI visualization of white matter lesions is pivotal for the diagnosis and management of multiple sclerosis (MS), the issue of detecting diffuse brain tissue damage beyond the apparent T2-hyperintense lesions continues to spark considerable interest. Motivated by the notion that rotating frame MRI methods are sensitive to slow motional regimes critical for tissue characterization, here we utilized novel imaging protocols of rotating frame MRI on a clinical 3 Tesla platform, including adiabatic longitudinal, T1ρ, and transverse, T2ρ, relaxation methods, and Relaxation Along a Fictitious Field (RAFF) in the rotating frame of rank 4 (RAFF4), in 10 relapsing-remitting multiple sclerosis patients and 10 sex- and age-matched healthy controls. T1ρ, T2ρ and RAFF4 relaxograms extracted from the whole white matter exhibited a significant shift towards longer relaxation time constants in MS patients as compared to controls. T1ρ and RAFF4 detected alterations even when considering only regions of normally appearing white matter (NAWM), while other MRI metrics such as T1w/T2w ratio and diffusion tensor imaging measures failed to find group differences. In addition, RAFF4, T2ρ and, to a lesser extent, T1ρ showed differences in subcortical grey matter structures, mainly hippocampus, whereas no functional changes in this region were detected in resting-state functional MRI metrics. We conclude that rotating frame MRI techniques are exceptionally sensitive methods for the detection of subtle abnormalities not only in NAWM, but also in deep grey matter in MS, where they surpass even highly sensitive measures of functional changes, which are often suggested to precede detectable structural alterations. Such abnormalities are consistent with a wide spectrum of different, but interconnected pathological features of MS, including the loss of neuronal cells and their axons, decreased levels of myelin even in NAWM, and altered iron content.

1. Introduction

More than a third of a century has elapsed since the first MRI studies of white matter lesions in multiple sclerosis (MS) patients (Lukes et al., 1983; Young et al., 1981), paving the path for the current role of MRI as a staple for MS diagnosis and monitoring (Filippi et al., 2016; Wattjes et al., 2015). Routine clinical practice is dominated by conventional MRI sequences such as T2-weighted imaging with fluid attenuated inversion recovery (FLAIR) and contrast-enhanced T1-weighted scans, which provide important, albeit limited information on subclinical disease activity and effectiveness of treatment. Notably, the derived measures such as T2 lesion load do not strongly correlate with the clinical findings of MS patients (Barkhof 2002) and neglect some aspects of central nervous system damage visible at the histological

Abbreviations: MRI, magnetic resonance imaging; DTI, diffusion tensor imaging; RAFF, relaxation along a fictitious field; MS, multiple sclerosis; DMT, disease modifying therapy; WM, white matter; NAWM, normal appearing white matter; DAWM, diffusely abnormal white matter; EDSS, Expanded Disability Status Scale; MSFC, Multiple Sclerosis Functional Composite; FSS, Fatigue Severity Scale; SDMT, Symbol Digits Modalities Test; CES-D, center for Epidemiologic Studies Depression Scale; MSQoL, Multiple Sclerosis Quality of Life-54; SD, standard deviation

* Corresponding author.
E-mail address: mangia@umn.edu (S. Mangia).

https://doi.org/10.1016/j.nicl.2020.102234
Received 4 July 2019; Received in revised form 16 February 2020; Accepted 29 February 2020
Available online 02 March 2020

level, calling for more sensitive MRI markers of microstructural injury accumulation and disease progression, even more so with the advent of new disease modifying therapies (DMT) (Torkildsen et al., 2016).

Substantial research efforts have been invested into the detection of alterations in grey matter (GM) (Burgetova et al., 2010; Cercignani et al., 2001; Crespy et al., 2011; Gracien et al., 2016; Sarchielli et al., 2002), impending plaques in the normal appearing white matter (NAWM) (Filippi et al., 1998; Tartaglia et al., 2002; Werring et al., 2000; Wiggermann et al., 2013; Wuerfel et al., 2004), and the recognition of subtle microstructural changes in the NAWM itself (Beer et al., 2016; Giannetti et al., 2014; Moll et al., 2011). Myelin reduction, axonal pathology and diffuse microglial activation in NAWM (Moll et al., 2011) are thought not only to contribute to the clinical picture, but to reflect the very nature of MS as a global inflammatory response in the whole brain originally stemming from a few focal flares of demyelination (Kutzelnigg et al., 2005). One way of addressing these issues is offered by quantitative MRI techniques, including magnetization transfer (MT) (Ropele and Fazekas 2009) and diffusion tensor imaging (DTI) (Cercignani and Wheeler-Kingshott, 2019). Although not commonly used in clinical practice, magnetization transfer ratio has been proven to correlate inversely with myelin loss, axonal damage (Schmierer et al., 2004) and disease severity measures (Traboulsee et al., 2003). Also, macromolecular proton fraction mapping provides direct measure of demyelination in the brain (Yarnykh 2012; Yarnykh et al., 2014). Diffusion tensor imaging (DTI) indices such as mean diffusivity (MD), fractional anisotropy (FA), axial diffusivity (AD) and radial diffusivity (RD) are sensitive to tissue integrity, axonal damage and myelin loss (Mottershead et al., 2003), and the reduced T2* relaxation time is thought to be associated with GM iron deposition as a sign of neurodegeneration in MS patients (Langkammer et al., 2010). Moreover, the ratio of T1-weighted and T2-weighted images (T1w/T2w ratio) has recently emerged as a viable candidate for the assessment of white matter (WM) injury in MS (Beer et al., 2016). Unfortunately, the reported differences in T1w/T2w ratio between healthy individuals and MS patients are subtle and require large sample sizes, impeding adoption of these techniques in clinical practice.

The emerging pharmacological methods specifically targeting selected pathways of MS pathology, such as drugs aimed at augmenting remyelination or preventing neurodegeneration, necessitate new approaches for monitoring microstructural disease activity (Wattjes et al., 2015). Several lines of theoretical and experimental evidence indicate that rotating frame quantitative MRI mapping techniques which utilize frequency swept pulses are valuable tools for tissue characterization in MS (Mangia et al., 2014) and other diseases (Mangia et al., 2017; Michaeli et al., 2007; Sierra et al., 2008; Nestrasil et al., 2010; Liimatainen et al., 2012). Whereas free-precession T1 and T2 relaxations due to dipolar interactions depend on magnetic field fluctuations at frequencies near the Larmor frequency in the MHz range, the rotating frame relaxations detect additional information from lower frequencies in the kHz range of the effective fields generated by the radio-frequency pulse. This inherent sensitivity of adiabatic T1ρ (Michaeli et al., 2006), T2ρ (Michaeli et al., 2004) and non-adiabatic RAFF (Relaxation Along a Fictitious Field) (Liimatainen et al., 2010) to slower motional regimes provides the ability to capture the large spectrum of water dynamics closely associated with the fine microstructure of various tissues. Indeed, the highly compartmentalized nature of WM consisting of axons, myelin sheaths and inter-axonal space, and the very character of MS disrupting myelin as the main barrier to inter-compartmental water exchange, demand acquisition protocols focused on slow motional regimes, as the mean residence time of myelin water protons varies in the range of hundreds of milliseconds to microsecond time scale (Dortch et al., 2013). Ergo, of particular relevance in this context is RAFFn (n standing for the rank of the rotating frame) due to the possibility of “fine-tuning” the contrast to different motional regimes and therefore tissue characteristics, as evidenced by the recent confirmation of RAFF4 and RAFF5 as a highly sensitive marker of myelin content (Hakkarainen et al., 2016; Satzer et al., 2015).

The overall goal of this cross-sectional study was to detect subtle abnormalities of multiple tissue types in patients with relapsing-remitting MS, including the whole WM, NAWM, diffusely abnormal WM (DAWM), cortical GM and subcortical GM. Towards this aim, we utilized imaging protocols of rotating frame MRI on a clinical 3 Tesla platform, in combination with DTI and conventional T1- and T2-weighted images as additional markers of microstructural damage, and resting-state functional MRI (rsfMRI) as a marker of functional impairment of relevant regions of interest. Based on our previous pilot study in MS patients (Mangia et al., 2014, 1), we hypothesised that both RAFF4 and T1ρ are able to detect significant differences between MS patients and controls, specifically in NAWM, superior to the capabilities of DTI and conventional protocols, including their derivatives as T1w/T2w ratio.

2. Methods

2.1. Subjects

Ten patients with relapsing-remitting MS diagnosed in accordance with the 2010 revised McDonald Criteria (Polman et al., 2011) were recruited from the University of Minnesota MS Clinic between June 2015 and April 2016. Demographic (sex, age) and basic neurologic data including disease history were obtained on the day of the MRI acquisition at the Center for Magnetic Resonance Research, complemented with the following quantitative measures: Expanded Disability Status Scale (EDSS), Multiple Sclerosis Functional Composite (MSFC), Fatigue Severity Scale (FSS), Symbol Digit Modalities Test (SDMT), center for Epidemiologic Studies Depression Scale (CES-D), and the Multiple Sclerosis Quality of Life-54 instrument (MSQOL). Additionally, we recruited ten frequency sex- and age-matched healthy controls. We did not include patients with a history of recent MS relapse or MS therapy change (within 6 months of enrollment), individuals with MRI contraindications, comorbid psychiatric or neurological disorder other than MS, or evidence of significant vascular or space occupying lesions in MRI scans.

This study was carried out in accordance with the recommendations of The Code of Federal Regulations. The protocol was approved by the Institutional Review Board: Human Subjects Committee of the University of Minnesota. A written informed consent was provided by each subject in accordance with the Declaration of Helsinki.

2.2. Imaging protocol

The MRI acquisition was performed using a 3 Tesla Siemens Prisma system. T1-weighted, T2-weighted images and DTI covered the whole brain. Magnetization-prepared rapid gradient-echo (MPRAGE) sequence was used for T1-weighted acquisitions, with the repetition time (TR) of 2150 ms, time to echo (TE) of 2.47 ms, inversion time (TI) of 1100 ms, voxel size of $1 \times 1 \times 1$ mm^3, flip angle of 8° and generalized autocalibrating partial parallel acquisition (GRAPPA) = 2. T2-weighted images were collected using the SPACE sequence, voxel size = $1 \times 1 \times 1$ mm^3, TE = 147 ms and GRAPPA = 2. Manufacturer-implemented pre-scan normalized algorithm was employed in both T1-weighted and T2-weighted scans. DTI datasets were acquired utilizing the following parameters: TR = 2820 ms, TE = 72.6 ms, multi band (MB) = 4, in 128 directions, with 5 additional non-diffusion weighted (b0) images, b-value = 1500 s/mm^2, voxel size = $1.8 \times 1.8 \times 1.8$ mm^3. The acquisitions were repeated with opposite phase encoding along the antero-posterior and postero-anterior axis. rsfMRI data was obtained using gradient echo Echo Planar Imaging (EPI) sequence, with TR = 900 ms, TE = 30 ms, and multi band factor = 4. Voxel size of $3 \times 3 \times 3$ mm^3 and matrix size of 64×64, 48 slices with interleaved slice acquisition was used to acquire 502 volumes in total. Rotating

frame relaxation measurements including adiabatic T1ρ, T2ρ and RAFF4 were obtained from 30 slices aligned to the anterior and posterior commissure and covering the whole supratentorial area and a part of the brainstem and cerebellum (voxel size = 1.6 × 1.6 × 3.6 mm^3, GRAPPA = 3, TE = 3.18 ms and TR = 2 s). The rotating frame MRI protocols have been described previously (Mangia et al., 2017). Briefly, hyperbolic secant pulses (Silver et al., 1984; Garwood and DelaBarre 2001) with adiabaticity factor R = 10, pulse duration = 6 ms, bandwidth BW = 1.3 kHz, peak power ${\omega_1}^{max}/(2\pi)$ = 800 Hz, and number of pulses = 0, 4, 8, 12, 16 MLEV phase cycled (Levitt et al., 1982) were used for adiabatic T1ρ and T2ρ measurements. For RAFF4 acquisitions, pulse duration was 4.56 ms, number of pulses = 0, 4, 8, 12, 16 and ${\omega_1}^{max}/(2\pi)$ = 327 Hz. Segmented gradient echo readout (2 segments) was used for imaging readout in all rotating frame relaxation measurements.

2.3. Image analysis

In the preliminary pre-processing step, manually defined masks of all T2-hyperintense WM lesions were used to reduce the intensity contrast within the WM lesion areas in T1w scans of MS subjects utilizing the previously published "lesion-filling" process (Battaglini et al., 2012). The aim of this procedure was to avoid incorrect automatic segmentation of juxtacortical MS lesions as GM in the subsequent analysis. Further analysis was performed using the human connectome project (HCP) minimal preprocessing pipeline (Glasser et al., 2013), consisting of the PreFreesurfer, FreeSurfer (FreeSurfer 5.3-HCP; http://surfer.nmr.mgh.harvard.edu/) and PostFreesurfer step for the structural data. The accuracy of the segmentation in each subject was visually inspected by a trained operator (P.F.). The PostFreesurfer step and all subsequent relevant analyses utilized the T1-weighted scan without the preliminary lesion correction so that correct T1w/T2w ratios were obtained for lesion areas.

The following masks for regions of interest (ROIs) were derived from the automatic labelling results in each subject: whole WM, cortical GM, basal ganglia, thalamus, hippocampus and amygdala. Furthermore, the whole WM was carefully segmented into three distinct WM types (NAWM, DAWM and lesions) utilizing a hybrid, semi-automatic approach, where two specific T2 intensity thresholds (distinguishing NAWM / DAWM and DAWM / lesions) were individually selected for each MS patient based on thorough visual evaluation by two neurologists (A.C., an MS specialist, and P.F.) in the normalized T2-weighted scans coregistered to the T1-weighted scan (see Fig. 1). For the purposes of this study, DAWM was considered WM with T2 intensity above the normal values expectable for healthy WM but still below intensities which were considered true lesions. This approach consistently identified DAWM in all MS patients. No further cluster thresholding or erosion of these masks were performed, as these steps introduced inconsistent results across individuals and did not improve a possible major concern of the interference of partial volume effects. Nonetheless, this concern was solved at a later step of processing during the coregistration of these masks to lower resolution images, where only coregistered voxels with an intensity of at least 0.9 after trilinear interpolation of the original binary WM masks were considered in further analyses (see the Supplementary figure 2 for visualisation). This value is generally recommended as a conservative threshold. The acquired MRI scans were not optimized for the detection of cortical GM lesions, so no corresponding GM segmentation was performed. T1w/T2w ratio as calculated in the HCP minimal preprocessing data was used in the subsequent analyses.

A 2-step 3D rigid body motion correction was performed in T1ρ, T2ρ and RAFF4 scans utilizing the MCFLIRT algorithm implemented in FSL 5.0.6 (Jenkinson et al., 2012, 2002). All acquired scans were co-registered to the first acquisition of the relevant sequence utilizing the default MCFLIRT parameters (6 degrees of freedom, trilinear interpolation and normalized correlation as cost function). It is important to emphasize that the contrasts of individual scans with rising numbers of pulses are at the borderline between the requirements for within-modality and between-modality cost functions, i.e. similar, but not completely identical as presumed for normalized correlation. However, both visual inspection of the coregistered scans and motion inspection (root-mean-squared voxel displacement) showed that MCFLIRT yielded a satisfactory result (motion less than one voxel). Afterwards, the relaxation time constants of individual sequences were calculated using custom routines based on the Aedes software package (http://aedes.uef.fi) in MATLAB R2016a (MathWorks, Inc., Natick, MA). 2-parameter non-linear fitting was used to estimate M0 and relaxation time in T1ρ and T2ρ acquisitions, and a 4-parameter non-linear fitting for M0, Mss (steady state value of magnetization), Mz (initial magnetization value measured from the negative hemisphere) and relaxation time for RAFF4 acquisitions. In the following step, T1ρ, T2ρ and RAFF4 maps were co-registered (3D rigid body co-registration) to the anatomical scan using the BB-register algorithm as implemented in FreeSurfer 6.0 with mri_robust_register initialisation (Reuter et al., 2010), to create co-registration matrices used in the subsequent steps for inverse co-registration of structural masks to these lower resolution images.

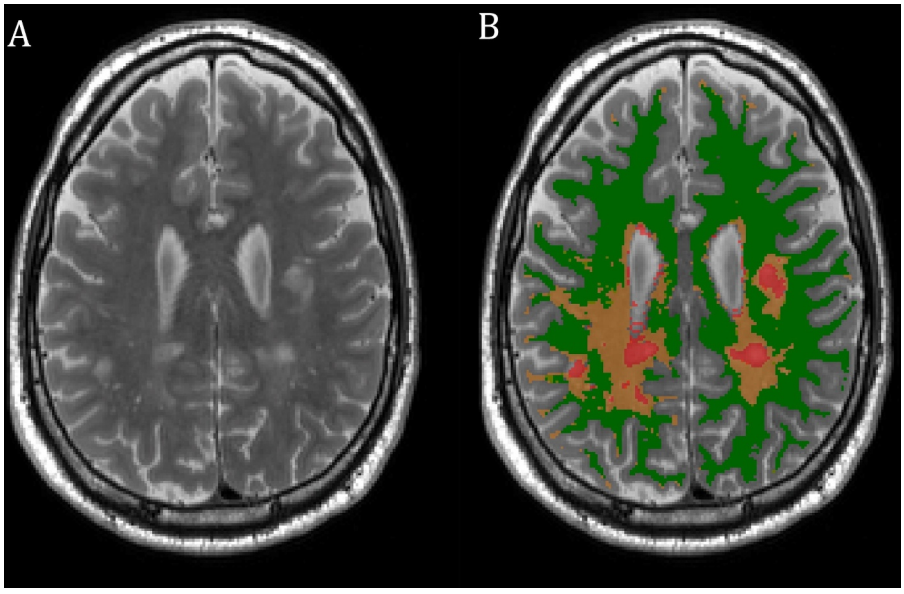

Fig. 1. Image slice from a representative MS subject: (A) native T2-weighted image depicting significant white matter (WM) abnormalities; (B) superimposed WM ROIs created by a semi-automated approach based on individual T2 intensity thresholds, including normal appearing WM (green), diffusely abnormal WM (brown) and lesions (red). Radiological laterality conventions (with the right side of the figure corresponding to the left side of the brain) are used.

Table 1
Demographics and clinical characteristics of all subjects. Scores provided as mean ± standard deviation (range). *EDSS* Expanded Disability Status Scale, *MSFC* Multiple Sclerosis Functional Composite, *FSS* Fatigue Severity Scale, *SDMT* Symbol Digit Modalities Test, *CES-D* centre for Epidemiologic Studies Depression Scale, *MSQoL* Multiple Sclerosis Quality of Life-54.

	Healthy controls	MS patients
N	10	10
Gender (female/male)	8/2	8/2
Age [years]	46.0 ± 13.4 (20–62)	47.3 ± 11.8 (19–59)
Disease duration [years]	–	12.1 ± 4.8 (5–17)
EDSS	–	2.7 ± 1.2 (1.0–4.0)
MSFC	–	0.28 ± 0.49 (0.79–0.84)
SDMT	–	52.9 ± 14.0 (35–83)
FSS	–	39.6 ± 14.2 (17–60)
CES-D	–	11.2 ± 9.4 (1–34)
MSQoL, physical section	–	65.7 ± 18.0 (35.2–86.1)
MSQoL, mental section	–	74.4 ± 15.7 (42.6–87.5)

DWI datasets were processed utilizing the HCP minimal preprocessing pipeline (Glasser et al., 2013), with subsequent diffusion tensor fitting to generate FA, MD, AD and RD (Andersson and Stamatios, 2016; Andersson et al., 2003). rsfMRI acquisitions were also analysed using the HCP minimal preprocessing pipeline followed by the HCP rsfMRI post-processing pipeline (Smith et al., 2013). HCP training data was used for the FIX auto-classification algorithm (Salimi-Khorshidi et al., 2014) with subsequent manual examination and amendments to the FIX-derived labelling of artefactual components before the regression of their contribution out of the rsfMRI data. The AFNI package (Cox, 1996) was utilized to calculate voxel-wise degree centrality (DeCe) and regional homogeneity (ReHo) based on the cleaned volumetric output of the pipeline.

Subsequently, the masks derived from automatic segmentation and semi-automatically created WM masks (NAWM, DAWM, and lesions) were co-registered to the images with lower resolution to avoid oversampling and the inherently associated obscurity. The inverse matrices created by 3D rigid body co-registration of T1ρ, T2ρ and RAFF maps to the T1-weighted scan were utilized and the resulting co-registrations of individual images and masks were visually inspected in every subject. Only voxels with a probability of inclusion in the relevant ROI of at least 0.9 were utilised in the subsequent image masking to avoid the "bleeding" of mixed information from adjacent voxels located at the interfaces of individual tissue types / ROIs.

2.4. Statistical analyses

Equivalence analysis (two one-sided tests) was used to confirm the absence of statistically significant differences (type I error = 0.05) in sex and age between the MS patients and healthy controls, with the differences of 33% and 10 years for sex and age considered clinically relevant. Quantitative clinical data were summarized using descriptive statistical approaches.

Means of the MRI metrics (adiabatic T1ρ, and T2ρ, RAFF4, FA, MD, AD, RD and T1w/T2w ratio; and DeCe and ReHo for GM masks only) were calculated within the individual ROIs per subject. Normality of these mean values was assessed with the Kolmogorov–Smirnov test per ROI. T1ρ, T2ρ, RAFF4, T1w/T2w ratio, FA, MD, AD and RD per-subject histograms were created for the whole WM ROI, separately for MS patients and controls, and per-subject skewness and kurtosis were calculated for these histograms to provide additional information about eventual between-group shape differences. Note that we refer to histograms of relaxation times as relaxograms.

Comparisons of MRI parameters were carried out between healthy controls whole WM and MS patients for each of whole WM, NAWM, DAWM, and WM lesions and between healthy controls and MS patients for each of cortical GM, basal ganglia, thalamus, amygdala, and hippocampus; two-tailed two-sample t-tests were used. A type I error rate of 0.05 was used after false discovery rate (FDR) correction for multiple modalities (8: T1w/T2w ratio, T1ρ, T2ρ, RAFF4, MD, FA, DeCe, ReHo) and ROIs (9). Separate FDR correction with was implemented for two-tailed two-sample t-tests of kurtosis and skewness, incorporating 6 modalities (T1w/T2w ratio, T1ρ, T2ρ, RAFF4, MD, FA) and 2 measures (kurtosis and skewness). Note that AD and RD were not included among the primary modalities due to their redundancy with FA and MD metrics. Pearson's correlation analysis was carried out to correlate individual clinical measures of interest (7: disease duration, EDSS, MSFC, SDMT, FSS, CES-D, MSQoL) with mean MRI parameter per ROI (9 ROIs, with the exception of rsfMRI measures, where 5 ROIs were considered, and 8 MRI parameters) with similar FDR correction.

2 scatter plots of mean T1ρ vs. mean T2ρ relaxation times were added to further elucidate the results: (1) scatterplot in whole WM to show the clustering of healthy controls and MS patients; and (2) scatterplot in segmented WM to show the clustering of NAWM, DAWM and lesions in MS patients.

Lastly, the volumes of 7 ROIs (WM, cortical GM, lateral ventricles, basal ganglia, thalamus, amygdala, hippocampus) and the volume of the whole brain, as provided by the automatic segmentation algorithm of FreeSurfer, were compared between the MS patients and healthy subjects using two-sided two-sample t-tests.

3. Results

3.1. Demographics

The two one-sided tests confirmed the equivalence of both sex and age distributions between the two study groups (sex, $p = 0.048$; age, $p = 0.030$, for MS subjects and healthy controls, respectively). Demographic information is provided in Table 1. The average disease duration of the MS group was 12.10 years (SD 4.82). Four MS patients reached EDSS stage 4 (gait impairment), the other six subjects ranged from 1 to 2 (without gait impairment). All MS subjects were on a stable DMT regimen: dimethyl fumarate – 4 subjects; glatiramer acetate – 2 subjects; natalizumab – 2 subjects; fingolimod and teriflunomide – 1 subject each. For further clinical information, see Table 1.

3.2. ROI masks

The mean thresholds for the individually created WM masks in MS patients based on T2-weighted signal intensities (see Fig. 1, numbers in a.u.) were 228.0 (range of 175–266) and 264.4 (range of 196–310) for the NAWM/DAWM and DAWM/lesion cut-offs, respectively. This considerable inter-subject variability and overlap of the ranges at the group level (perceived even in T2-weighted images processed using the prescan normalization implemented by the MRI scanner manufacturer) precludes determining any simple numeric cut-off value plausible for all the MS subjects. All the created NAWM, DAWM, and lesion masks were manually inspected (A.C., an MS specialist, and P.F.), but no further local manual corrections were performed. Although this approach also labelled juxtacortical WM voxels with slightly increased intensities in some areas as DAWM, it was not possible to truly differentiate between partial volume effects due to insufficient resolution and juxtacortical lesions.

Kolmogorov–Smirnov tests confirmed the absence of significant deviations from the normal distribution ($p > 0.05$) for the averages of voxel values for individual MRI sequences and all ROIs with sufficient number of voxels, enabling us to use parametric statistical methods. However, normality could not be confirmed for the lesional WM masks in lower resolution methods, so not only the paucity of values, but also the distribution of relevant values in these areas, call for caution in eventual interpretation of borderline results.

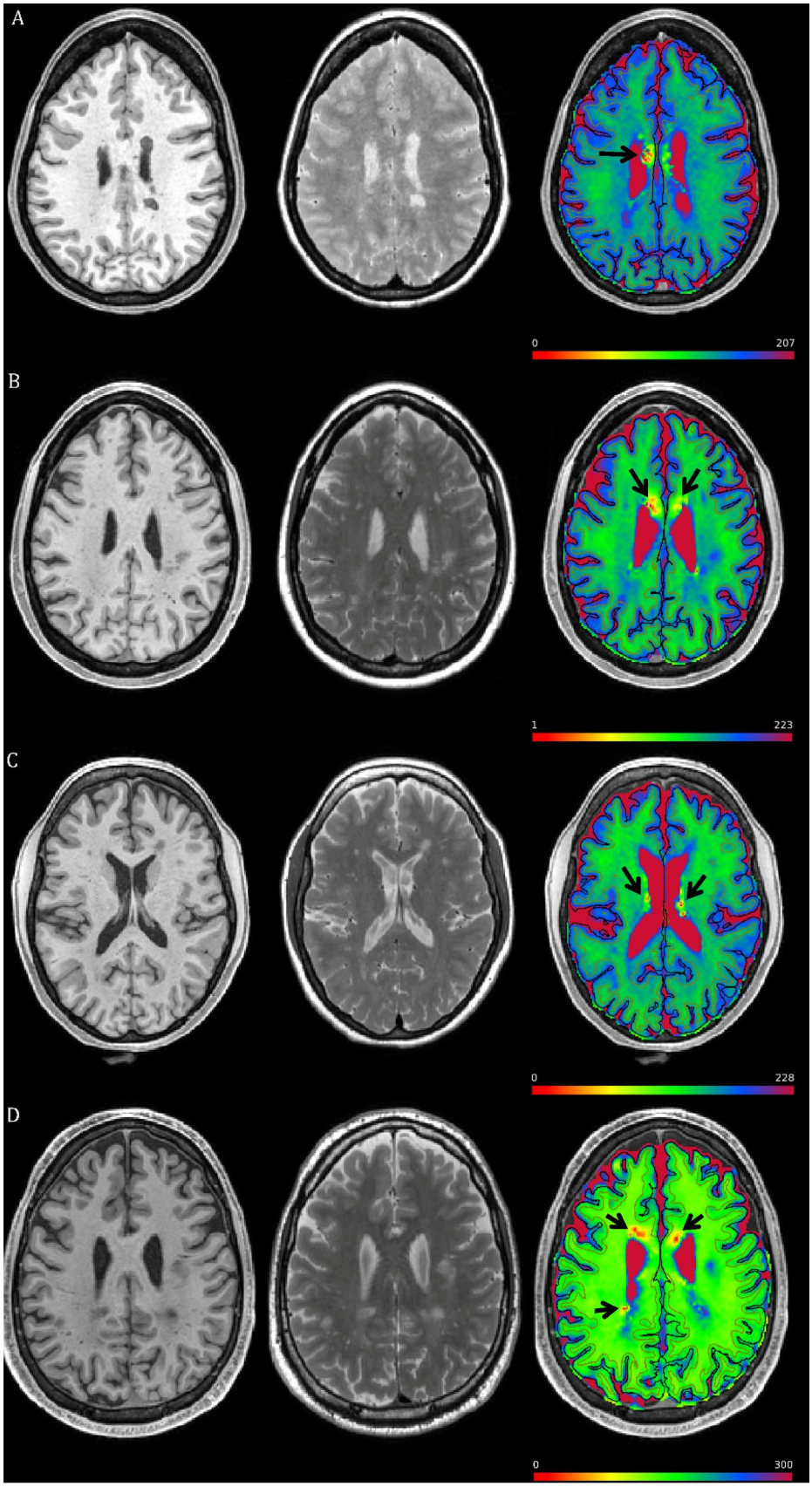

Fig. 2. T1-weighted (left), T2-weighted (middle) and T1ρ (right) images with reconstructed surfaces for better orientation of 4 MS subjects with conspicuous T1- and T2-negative T1ρ lesions in the periventricular white matter (A and B), in the bilateral thalami (C) and in the genu of corpus callosum (D). The MS subject in (D) had also a similar lesion in the head of the right caudate (not depicted). Black arrows point to the lesions of interest. The scales denote relaxation time in [ms]. Radiological laterality conventions (with the right side of the figure corresponding to the left side of the brain) are used. The dark regions in the cerebrospinal fluid in the T2-weighted images are probably caused by the inherent susceptibility of the T2-weighted scans to the loss of phase in highly heterogeneous substances and possibly flow changes, sometimes described as “flow void”.

Table 2
MRI metrics in the regions of interest. *T*-test, false discovery rate corrected for multiple modalities (6 for white matter and 8 for grey matter) and ROIs (9). Statistically significant results ($p < 0.05$, corrected) are marked in bold italics. For AD and RD, no FDR correction is provided, as these are only included for completeness and mirror their compound variable – MD. Positive *T*-values denote higher values of respective parameters in MS patients. WM: white matter; NAWM: normal appearing WM; DWM: "dirty" WM.

MRI metric	Region of Interest	Controls (mean ± SD, $n = 10$)	MS patients (mean ± SD, $n = 10$)	difference (patients minus controls)	*T*-value	*p*-value, uncorr	*p*-value, FDR-corr
RAFF4 [ms]	Whole WM	253 ± 7	269 ± 9	6.4%	4.63	0.0002	***0.0011***
	NAWM	253* ± 7*	262 ± 7	3.5%	2.88	0.0099	***0.0317***
	DWM	253* ± 7*	266 ± 8	5.3%	3.94	0.0010	***0.0038***
	WM lesions	253* ± 7*	356 ± 41	40.9%	7.88	0.0000	***0.0000***
	Thalamus	272 ± 8	278 ± 7	2.1%	1.74	0.0987	0.1707
	Amygdala	329 ± 12	338 ± 7	2.6%	1.91	0.0717	0.1391
	Hippocampus	314 ± 10	328 ± 7	4.5%	3.62	0.0019	***0.0069***
	Basal ganglia	296 ± 8	305 ± 10	3.0%	2.16	0.0449	0.0991
	Cortex	334 ± 9	342 ± 8	2.3%	2.06	0.0545	0.1163
T1ρ [ms]	Whole WM	131 ± 5	142 ± 4	8.1%	5.59	0.0000	***0.0002***
	NAWM	131* ± 5*	136 ± 2	3.3%	2.64	0.0167	***0.0485***
	DWM	131* ± 5*	146 ± 4	11.2%	7.25	0.0000	***0.0000***
	WM lesions	131* ± 5*	203 ± 24	54.4%	9.27	0.0000	***0.0000***
	Thalamus	146 ± 4	149 ± 1	2.0%	2.29	0.0341	0.0840
	Amygdala	170 ± 5	172 ± 4	1.2%	1.03	0.3156	0.4489
	Hippocampus	166 ± 3	172 ± 7	4.0%	2.73	0.0137	***0.0417***
	Basal ganglia	148 ± 3	152 ± 4	2.5%	2.36	0.0297	0.0761
	Cortex	163 ± 3	166 ± 4	1.6%	1.85	0.0808	0.1520
T2ρ [ms]	Whole WM	71 ± 2	75 ± 3	6.2%	4.25	0.0005	***0.0024***
	NAWM	71* ± 2*	71 ± 2	0.4%	0.32	0.7490	0.8560
	DWM	71* ± 2*	80 ± 3	13.3%	7.89	0.0000	***0.0000***
	WM lesions	71* ± 2*	113 ± 14	59.4%	9.52	0.0000	***0.0000***
	Thalamus	72 ± 1	73 ± 2	1.6%	1.55	0.1389	0.2279
	Amygdala	88 ± 2	89 ± 2	1.6%	1.99	0.0618	0.1236
	Hippocampus	86 ± 2	89 ± 2	3.8%	4.03	0.0008	***0.0036***
	Basal ganglia	66 ± 2	66 ± 3	1.0%	0.60	0.5545	0.6824
	Cortex	80 ± 2	81 ± 2	1.4%	1.31	0.2074	0.3238
T1w/T2w ratio	Whole WM	1.21 ± 0.06	1.13 ± 0.05	−6.7%	−3.12	0.0059	***0.0197***
	NAWM	1.21* ± 0.06*	1.15 ± 0.05	−5.1%	−2.41	0.0271	0.0723
	DWM	1.21* ± 0.06*	0.86 ± 0.07	−29.1%	−11.95	0.0000	***0.0000***
	WM lesions	1.21* ± 0.06*	0.61 ± 0.08	−49.3%	−17.87	0.0000	***0.0000***
	Thalamus	1.22 ± 0.04	1.20 ± 0.06	−1.6%	−0.83	0.4175	0.5463
	Amygdala	0.80 ± 0.03	0.79 ± 0.02	−2.3%	−1.67	0.1128	0.1899
	Hippocampus	0.81 ± 0.03	0.78 ± 0.03	−3.6%	−2.52	0.0216	0.0601
	Basal ganglia	1.16 ± 0.05	1.14 ± 0.08	−1.7%	−0.65	0.5208	0.6535
	Cortex	0.80 ± 0.03	0.78 ± 0.03	−2.0%	−1.14	0.2705	0.3935
FA	Whole WM	0.50 ± 0.02	0.48 ± 0.02	−4.2%	−2.22	0.0396	0.0938
	NAWM	0.50* ± 0.02*	0.48 ± 0.02	−3.5%	−2.04	0.0565	0.1167
	DWM	0.50* ± 0.02*	0.43 ± 0.04	−14.1%	−4.78	0.0002	***0.0009***
	WM lesions	0.50* ± 0.02*	0.31 ± 0.05	−38.3%	−10.92	0.0000	***0.0000***
	Thalamus	0.34 ± 0.02	0.35 ± 0.03	3.9%	1.32	0.2043	0.3238
	Amygdala	0.17 ± 0.01	0.18 ± 0.02	5.3%	1.18	0.2548	0.3792
	Hippocampus	0.14 ± 0.02	0.13 ± 0.01	−7.2%	−1.81	0.0877	0.1600
	Basal ganglia	0.18 ± 0.02	0.19 ± 0.03	5.6%	0.97	0.3449	0.4798
	Cortex	0.14 ± 0.01	0.14 ± 0.01	−0.5%	−0.23	0.8191	0.8885
MD x 10^{-3} [mm^2/s]	Whole WM	0.63 ± 0.02	0.66 ± 0.03	5.7%	3.68	0.0017	***0.0065***
	NAWM	0.63* ± 0.02*	0.63 ± 0.02	−0.2%	−0.18	0.8566	0.8987
	DWM	0.63* ± 0.02*	0.69 ± 0.05	9.8%	3.99	0.0009	***0.0036***
	WM lesions	0.63* ± 0.02*	1.07 ± 0.15	70.5%	9.12	0.0000	***0.0000***
	Thalamus	0.65 ± 0.01	0.65 ± 0.02	0.7%	0.70	0.4901	0.6273
	Amygdala	0.71 ± 0.02	0.71 ± 0.02	−0.1%	−0.12	0.9085	0.9229
	Hippocampus	0.75 ± 0.02	0.77 ± 0.02	2.5%	2.16	0.0442	0.0991
	Basal ganglia	0.64 ± 0.02	0.64 ± 0.02	0.1%	0.08	0.9394	0.9394
	Cortex	0.67 ± 0.01	0.67 ± 0.01	0.7%	0.90	0.3783	0.5151
AD x 10^{-3} [mm^2/s]	Whole WM	1.042 ± 0.02	1.077 ± 0.02	3.4%	4.07	0.0007	N/A
	NAWM	1.042* ± 0.02*	1.032 ± 0.02	−1.0%	−1.07	0.3005	N/A
	DWM	1.042* ± 0.02*	1.121 ± 0.05	7.6%	5.01	0.0001	N/A
	WM lesions	1.042* ± 0.02*	1.513 ± 0.19	45.2%	7.66	0.0000	N/A
	Thalamus	0.896 ± 0.01	0.912 ± 0.02	1.8%	2.44	0.0255	N/A
	Amygdala	0.855 ± 0.03	0.864 ± 0.03	1.1%	0.73	0.4720	N/A
	Hippocampus	0.889 ± 0.03	0.903 ± 0.02	1.6%	1.25	0.2274	N/A
	Basal ganglia	0.768 ± 0.03	0.776 ± 0.03	1.0%	0.75	0.4646	N/A
	Cortex	0.818 ± 0.02	0.823 ± 0.01	0.6%	1.03	0.3151	N/A

(*continued on next page*)

Table 2 (*continued*)

MRI metric	Region of Interest	Controls (mean ± SD, n = 10)	MS patients (mean ± SD, n = 10)	difference (patients minus controls)	T-value	p-value, uncorr	p-value, FDR-corr
RD x 10^{-3} [mm^2/s]	Whole WM	0.439 ± 0.02*	0.477 ± 0.03	8.7%	3.21	0.0048	N/A
	NAWM	0.439* ± 0.02*	0.452 ± 0.02	3.0%	1.36	0.1916	N/A
	DWM	0.439* ± 0.02*	0.528 ± 0.06	20.3%	4.65	0.0002	N/A
	WM lesions	0.439* ± 0.02*	0.914 ± 0.15	108.2%	9.98	0.0000	N/A
	Thalamus	0.531 ± 0.01	0.53 ± 0.03	−0.2%	−0.17	0.8662	N/A
	Amygdala	0.658 ± 0.02	0.652 ± 0.02	−0.9%	−0.72	0.4787	N/A
	Hippocampus	0.71 ± 0.02	0.732 ± 0.02	3.1%	2.59	0.0184	N/A
	Basal ganglia	0.588 ± 0.02	0.587 ± 0.02	−0.2%	−0.09	0.9291	N/A
	Cortex	0.65 ± 0.01	0.656 ± 0.01	0.9%	0.95	0.3530	N/A
Degree Centrality	Thalamus	−0.264 ± 0.196	−0.134 ± 0.120	−49.3%	1.79	0.0900	0.1600
	Amygdala	−0.498 ± 0.173	−0.533 ± 0.269	7.1%	−0.35	0.7319	0.8560
	Hippocampus	−0.186 ± 0.215	−0.213 ± 0.210	14.1%	−0.28	0.7860	0.8825
	Basal ganglia	−0.329 ± 0.236	−0.224 ± 0.138	−32.1%	1.22	0.2376	0.3620
	Cortex	0.089 ± 0.036	0.092 ± 0.041	3.7%	0.19	0.8518	0.8987
Regional Homogeneity	Thalamus	0.142 ± 0.020	0.138 ± 0.021	−2.8%	−0.43	0.6751	0.8152
	Amygdala	0.123 ± 0.021	0.120 ± 0.017	−2.4%	−0.34	0.7371	0.8560
	Hippocampus	0.134 ± 0.017	0.127 ± 0.017	−4.7%	−0.83	0.4182	0.5463
	Basal ganglia	0.153 ± 0.015	0.151 ± 0.019	−1.2%	−0.24	0.8096	0.8885
	Cortex	0.262 ± 0.048	0.259 ± 0.047	−0.96%	−0.12	0.9072	0.9229

* since controls did not have MS pathology, the value used for the group comparison is the same as for the whole WM.

3.3. T1ρ focal abnormalities

Visual inspection of the processed scans revealed multiple conspicuous T1ρ focal abnormalities in 4 MS patients (out of 10) (see Fig. 2), while no healthy controls showed comparable findings. Interestingly, no other sequence, including the T2-weighted images, detected any corresponding lesions in these areas (mostly WM in the vicinity of the lateral ventricles, namely several parts of the corpus callosum, but also caudate and thalamus). Notably, while T2-hyperintense lesions displayed prolonged relaxation time constants in T1ρ maps, the T1ρ relaxation time constants in these focal abnormities were substantially shorter. As the true nature of these T1ρ focal abnormalities is unclear as of now, no further changes in the T2w-based NAWM masks were performed to exclude these regions. Nonetheless, due to the scarcity of these abnormalities, even excluding these areas from NAWM masks resulted in negligible numerical differences in the averages and standard deviations beyond the precision of values provided in the Table 2.

3.4. Comparison of rotating frame relaxation protocols with other modalities

The T1ρ and T2ρ relaxation time constants (Table 2) were in line with our previous reports (Mangia et al., 2017, 2014). All the rotating frame methods were able to detect differences between the healthy controls whole WM and MS patients whole WM. T1ρ and RAFF4 additionally detected differences between healthy controls whole WM and each of the 3 segmented WM ROIs (NAWM, DAWM, WM lesions) for MS patients (Table 2). Specifically, there was a significant shift of the relaxograms in MS patients to longer relaxation times in T1ρ, T2ρ, and RAFF4 (Fig. 3). In NAWM, there was a significant relaxation prolongation in both T1ρ and RAFF4 as compared to healthy controls' whole WM. Although T1w/T2w ratio and MD detected certain differences in the whole WM masks, these methods were unable to distinguish the two groups in the NAWM mask. DAWM mean relaxation times (T1ρ, T2ρ and RAFF4) in MS patients were once again significantly longer than in the WM of healthy controls. Mean differences in DAWM as compared to healthy control WM were also picked up by the T1w/T2w ratio, FA and MD. Lastly, all the MRI protocols relevant for WM confirmed significant changes between the respective parameters in WM lesions of MS patients and whole WM of healthy controls. For details, see Table 2.

Analogous analyses, which included also rsfMRI parameters, were performed for cortical GM and several subcortical regions. Only T1ρ, T2ρ and RAFF4 were able to reveal statistically significant results, namely prolonged relaxation time constants in hippocampus (Table 2). No further cortical or subcortical GM differences were found between MS and controls. Interestingly, these microstructural changes were not reflected at the macrostructural level, as no significant differences in GM volume were found (see Supplementary Table 1).

3.5. Histogram and scatterplot analyses

The relaxograms of whole WM for healthy subjects and MS patients exhibit a clear shift of the mode towards longer relaxation time constants in T1ρ and RAFF in MS patients (Fig. 3). Additional histograms of DTI metrics and T1w/T2w ratio are presented in Fig. 4. While there were substantial MS-related deformations of T1ρ and T2ρ relaxograms, as reflected visually and in significant differences in kurtosis and skewness ($p < 0.01$ for both kurtosis and skewness in both T1ρ and T2ρ; see Table 3), the shapes of RAFF relaxograms in MS patients and healthy controls exhibited substantial similarities (neither kurtosis, nor skewness between-group differences were found, $p > 0.20$). Furthermore, the group difference relaxograms shown in Fig. 3 clearly confirm the shift of the above described relaxograms, with the peak differences in the relaxation time constants observed at about 70 ms, 130 ms, and 240 ms in T2ρ, T1ρ and RAFF4, respectively. Note that there is a trend of broader histograms also for MD and RD in MS patients (Fig. 4), however kurtosis differences did not reach significance for either MD (see Table 2) or RD (data not shown).

The scatterplot analysis (Fig. 5A) presents an appreciable clustering of the two subject groups, allowing us to estimate a T1ρ cut-off line of about 137 ms. Fig. 5B shows a clear separation between the ROI-averaged values for NAWM, DAWM and lesional WM in MS patients. Finally, the correlation analysis of individual clinical parameters of interest with mean ROI values for relevant MRI metrics failed to provide any significant findings.

4. Discussion

Building on our previous pilot study utilizing rotating frame relaxation parameters for the characterization of NAWM of MS (Mangia et al., 2014), here we extended the imaging protocol to a clinically relevant platform (3 Tesla), to multi-slice acquisitions for extensive brain coverage, and to the inclusion of RAFF4, a measure exceptionally sensitive to myelin content (Satzer et al., 2015). In

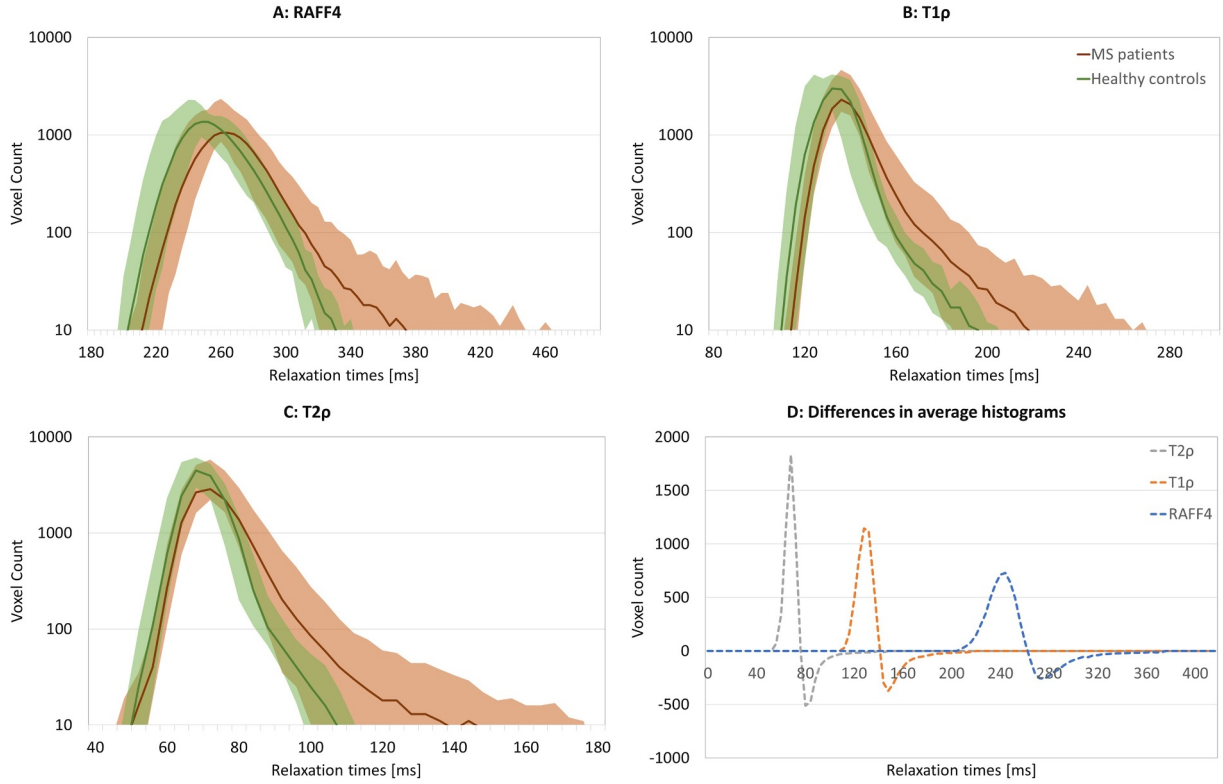

Fig. 3. Relaxograms of white matter (WM) MRI parameters RAFF4 (A), T1ρ (B), and T2ρ (C). Logarithmic *y*-axis scale (voxel count) and linear *x*-axis scale (relaxation parameter). Lines correspond to average values and shadows to ranges in the respective groups. Healthy controls depicted in green, MS patients in red. Furthermore, the group differences in average relaxogram (healthy controls minus MS patients) are shown (D), providing further information on the character of the observed relaxogram shift and maxima/minima of differences. (For interpretation of the references to color in this figure legend, the reader is referred to the web version of this article.)

general, the currently presented findings confirmed the ability of rotating frame methods to detect abnormalities of the NAWM and also GM structures, where well-established DTI metrics seem to fail. The calculation of the relaxograms for the various MRI metrics provided a robust characterization of the regions of interest which goes beyond what can be implicated by the mean values alone. This approach indeed enabled us to appreciate more delicate changes as skewness and kurtosis alterations in T1ρ and T2ρ WM relaxograms together with a shift to longer relaxation times, presumably reflecting a combination of diffuse WM changes and focal effects leading to the deformation of the right-side tail of the relaxogram. This notion is of major interest considering the ability of T1ρ to distinguish also general MS-related changes in NAWM, contrary to T2ρ. On the other hand, the simple shift of RAFF4 WM relaxogram to longer relaxation times without any shape deformation and its sensitivity to NAWM changes points to a rather unique ability of rotating frame protocols, when used in combination, to distinguish MS changes of diverse nature.

In the light of the previously demonstrated sensitivity of T1ρ to neuronal cellular density (Michaeli et al., 2007, 2009) and T2ρ to iron levels (Mitsumori et al., 2009; Michaeli et al., 2007), the interpretation of these alterations may not be as straightforward as in RAFF4, which strongly correlates with the myelin content (Satzer et al., 2015). Interestingly, the ability of rotating frame relaxation protocols implemented in this study to detect different, although partly overlapping motional regimens, beyond the spectrum of imaging methods widely used in clinical practice, might be reflected in different and relevant aspects of WM changes. The prolongation of T2ρ relaxation in the whole WM, accentuated in DAWM, corroborate well with current theories of iron level dysregulation in MS and its depletion in WM, mainly in chronic lesions (Stephenson et al., 2014). Considering the crucial importance of iron levels for maintaining proper function of enzymatic systems essential for oligodendrocyte progenitor cells and hence remyelination, the ability to monitor its concentration might prove of paramount importance for newer generations of DMTs (Green et al., 2017; Rae-Grant et al., 2018). Moreover, it is rather tempting to hypothesize that T1ρ relaxation prolongation in NAWM, a marker related to neuronal density as confirmed by histological studies in animals (Michaeli et al., 2009), should capture axonal degeneration, corroborated by the RAFF4 changes in both NAWM and whole WM ROIs. Furthermore, T1ρ, T2ρ and RAFF4 were able to identify significant differences from controls in hippocampus – a deep grey matter structure of paramount importance for the clinical condition and well-being of each MS patient. These findings may yet prove to be of utmost relevance for the detection of early MS changes, as even rsfMRI measures, previously often hypothesized as early markers of impeding structural alterations in MS patients (Faivre et al., 2016; Rocca et al., 2016; Chen et al., 2018), failed to find any between-group differences in our study.

4.1. T1ρ focal abnormities

Furthermore, the unique focal T1ρ abnormities which appeared as faster T1ρ relaxation and were undetectable by other MRI protocols, were observed in several MS patients, but not in healthy controls, and raise several intriguing questions. Not only the nature of pathology leading to these changes is of major interest, but also the implications of highly suspected lesions merit further research, as the current clinical MRI protocols and even several rotating frame relaxation methods such as RAFF4 and T2ρ are blind to them. In fact, the ability of a relaxation method to detect changes in tissue properties ultimately requires inherent sensitivity to the relevant relaxation channels while avoiding excessive shortening (or lengthening) of the relaxation time to avoid

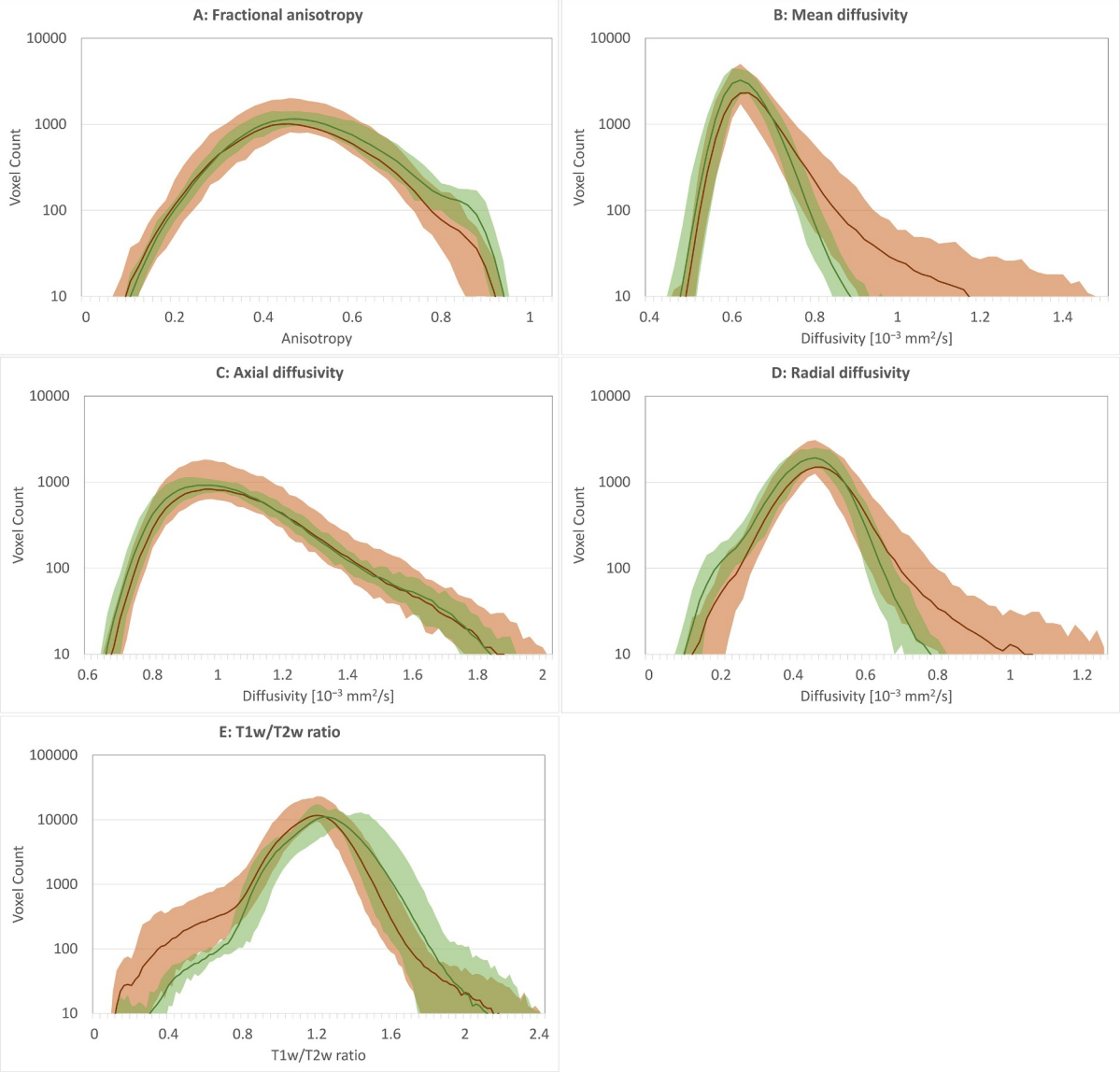

Fig. 4. Histograms of diffusion tensor imaging parameters [fractional anisotropy (FA), mean diffusivity (MD), axial diffusivity (AD) and radial diffusivity (RD)] and T1w/T2w ratio in white matter (WM). Logarithmic *y*-axis scale (voxel count), linear *x*-axis scale (individual parameters). Lines correspond to average values and shadows to ranges in the respective groups. Healthy controls depicted in green, MS patients in red. (For interpretation of the references to color in this figure legend, the reader is referred to the web version of this article.)

compromising accurate signal detection. As we have demonstrated previously, short T1ρ relaxation in tissue could arise from a pool of spins experiencing dipolar interactions with short correlation time, in the range of tens of nanoseconds or less, indicative of restricted mobility (Mangia et al., 2009). Notably, the T2ρ of these spins with restricted mobility would be even shorter than T1ρ. If such spins are also in exchange with free-like moving spins at a different chemical shift (due for instance to the presence of iron) and since the dynamic range of T2ρ is greater than T1ρ, the resulting anisochronous exchange –induced relaxation would not significantly affect T1ρ, but would make T2ρ as well

Table 3
Between-person averages of within-ROI histogram kurtosis and skewness for respective parameters in MS patients and healthy controls in whole white matter. *T*-test, false discovery rate corrected for multiple modalities (6) and histogram shape measures (2). Statistically significant results ($p < 0.05$, corrected) are marked in bold italics. Positive *T*-values denote higher values of respective parameters in MS patients.

	Average Kurtosis				Average Skewness			
	Healthy controls	MS patients	*t*-value	*p*	Healthy controls	MS patients	*t*-value	*p*
RAFF4	20.44	19.79	−0.692	0.594	4.21	4.14	−0.730	0.594
T1ρ	37.32	30.74	−3.915	***0.003***	5.80	5.21	−4.137	***0.003***
T2ρ	18.66	13.77	−4.475	***0.002***	4.02	3.40	−4.593	***0.002***
T1w/T2w ratio	130.66	122.47	−1.113	0.421	10.93	10.40	−1.753	0.166
FA	2.06	2.08	0.343	0.735	0.73	0.75	0.618	0.594
MD	23.20	20.13	−1.849	0.162	4.49	4.15	−1.966	0.156

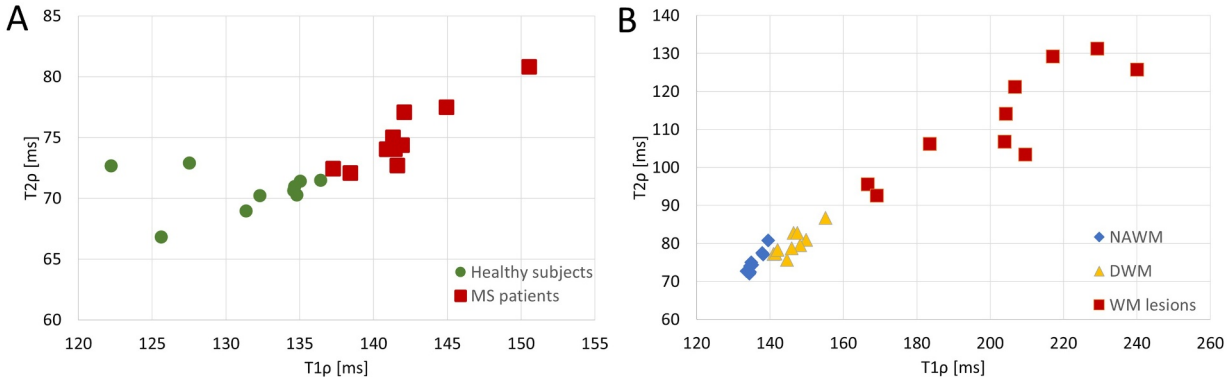

Fig. 5. Scatter plots, displaying mean T1ρ (*x*-axis) and mean T2ρ (y-axis) relaxation times of (A) white matter (WM) in healthy controls (green dots) and MS patients (red squares); and (B) normal appearing WM (NAWM) (blue diamonds), diffusely abnormal WM (yellow triangles) and lesions (red squares) in MS patients. Both (A) and (B) show significant clustering tendencies. (For interpretation of the references to color in this figure legend, the reader is referred to the web version of this article.)

as T2 so short that could escape detection in T2ρ and T2 acquisitions. On the other hand, RAFF4 relaxation times generally become substantially shorter in presence of more restricted motions than those shortening adiabatic T1ρ (Hakkarainen et al., 2016), and they are not significantly impacted by fast exchange especially if the periodicity of RAFF4 irradiation is not tuned to the difference in chemical shifts of the two pools (Liimatainen et al., 2018). These qualitative arguments demonstrate the importance for rotating frame relaxation techniques to be tuned to the relevant regimes of motion, and explain why some lesions may appear in T1ρ, but not in T2ρ, T2 or RAFF4 acquisitions. Nonetheless, all these parameters likely provide complementary information on NAWM/WM changes encompassing multiple factors, including factors relevant to disease pathology, and also perhaps associated with tissue characteristics not affected by MS. There were no differences in the clinical characteristics of MS patients with and without these focal T1ρ abnormities. However, as there were no comparable findings in any healthy controls and considering our previous studies showing T1ρ abnormalities in MS patients (Mangia et al., 2017), these findings are intriguing in terms of T1ρ providing a novel non-invasive method for detecting CNS pathology in MS. Although an artefactual explanation for these "lesions" cannot be completely excluded, the size, shape and location of them are completely consistent with the well-established CNS pathology of MS. Further studies will be necessary to elucidate this issue fully.

4.2. Comparison of rotating frame relaxation protocols with other modalities

Other modalities such as DTI (Schmithorst et al., 2002), magnetization transfer (Ropele and Fazekas 2009), T1w/T2w ratio (Beer et al., 2016) or multi-exponential T2 (McCreary et al., 2009) have the potential to assess tissue organization as well. However, the specificity of DTI measures to the underlying macroscopic-level organization of fibres was not a marker sufficient to provide results comparably significant to the approaches based on rotating frame relaxation in our study. FA and MD indeed failed to reach statistical significance in NAWM ROIs, while FA revealed relevant differences only in the areas previously marked as suspicious based on the T2-weighted intensities. Furthermore, even though T1w/T2w ratio in WM was previously reported in MS studies (Beer et al., 2016), it may not necessarily reflect the content or integrity of myelin (Uddin et al., 2018), lacking histological studies except for cortical regions (Glasser and Van Essen 2011). It is nonetheless a parameter exhibiting plausible ability to detect WM changes in MS and as such definitely deservers further attention. All in all, the main objective of the presented study – to show the superiority of the novel rotating frame MRI protocols to the commonly used metrics as DWI, T1w/T2w ratio for white matter and rsfMRI metrics for grey matter has been clearly met. Interestingly, rotating frame MRI protocols were the only ones able to detect any GM changes, surpassing functional MRI metrics, even though functional connectivity changes are often thought to precede MRI-detectable structural changes.

The promises of advanced quantitative MRI techniques have not been actualized in clinical practice yet, where T2-weighted and contrast-enhanced T1-weighted MRI scans remain the modalities of choice for monitoring clinically silent disease progression and detection of acute inflammation (Massimo Filippi et al., 2016; Wattjes et al., 2015). These "traditional" approaches unfortunately fail to provide information possibly integral to MS clinical management like early detection of microstructural changes and more specific subclinical disease progression, with the ultimate goal to evaluate the response to advanced therapeutic regimens. Despite the promising results, one limitation of the current study is the absence of validation in a longitudinal manner and between individual MS centres. Because of the cross-sectional design, we are not able to provide further information on the stability of parameters in individual subjects over time, even though the narrow inter-subject range of values would suggest favourable prospects in this regard. Further study on the temporal evolution in a cohort larger than in the present study would likely shed light on this matter and would avoid problems inherently associated with higher number of metrics and statistical analyses in a smaller cohort of subjects as is the case in the currently presented study. In addition, integration of the current imaging protocols into general practice might be partially limited by the length of the acquisition protocol (about 20 min for all three rotating frame relaxation measurements) and the relatively low spatial resolution. On a positive note, both limitations may be solved using faster readout schemes and parallel acquisition protocols. Secondly, the semi-automatic approach implemented in the differentiation of NAWM, DAWM and lesions with fixed thresholds is associated with a risk of several artefact types (e.g. the inclusion of juxtacortical WM voxels into DAWM mask). However, these small problematic regions are not reflected in the relevant ROI analyses due to the lower resolution of rotating frame and DWI protocols and the conservative thresholding of coregistered ROI masks. All in all, this approach provided the most reasonable NAWM, DAWM and lesion masks as the thresholds of T2w intensities corresponding to DAWM and lesions were chosen by an experienced MS specialist. Finally, it is worth mentioning that motion artefacts did not appear to be a problem which may have compromised data quality, as confirmed by the very tight distribution of relaxation values in healthy controls. Despite the relatively low resolution implemented here, the rotating frame relaxations provided valuable information on WM characteristics, to the extent allowing for differentiation between healthy and MS subjects based on both T1ρ and T2ρ

relaxation times with viable sensitivity and specificity of the chosen threshold; however, validation in a much larger cohort is warranted.

5. Conclusions

Taken together, the rotating frame relaxation techniques demonstrated the ability to detect abnormalities not only in WM and specifically NAWM, but also in deep grey matter, possibly describing a wide spectrum of different, albeit interconnected pathological features of MS, including the loss of neuronal cells and their axons, decreased levels of myelin even in NAWM, and reduced iron content. Ergo, these methods hold promise as potential non-invasive tools for monitoring MS activity and eventually for the evaluation of therapeutic effects, even though substantial efforts will need to be invested to ensure the implementation, harmonization and full interpretation of rotating frame relaxation protocols for clinical practice in MS.

Author contributions

Pavel Filip, Alena Svatkova, Adam F Carpenter, Lynn E Eberly, Igor Nestrasil, Mikko J Nissi, Shalom Michaeli, Silvia Mangia

PF participated in analysis and interpretation of the data, and preparing the manuscript. AS participated in analyses and editing the manuscript. AFC participated in design of the work, acquisition, analyses and interpretation of the data, and editing the manuscript. LEE participated in analyses of data, and editing the manuscript. IN participated in interpretation of the data, and editing the manuscript. MJN participated in analyses and interpretation of the data, and editing the manuscript. SMi participated in design of the work, acquisition and analysis of the data, interpretation of the data, funding acquisition, and editing the manuscript. SMa participated in design of the work, acquisition, analysis and interpretation of the data, funding acquisition and preparing the manuscript.

Declaration of Competing Interest

There are no potential conflicts of interests regarding this paper and no financial or personal relationships that might bias this work.

Acknowledgments and funding

The authors are grateful to the patients and their families for their support of research activities. The authors are also grateful to Wendy Elvendahl for assistance with MRI acquisitions, Krista Mullen for subject recruitment, and Petr Bednarik for assistance with developing post-processing code.

This work was supported by the EUH2020 Marie Skłodowska RISE project #691110 (MICROBRADAM), by the University of Minnesota Foundation, and by the National Institutes of Health (Funding P41 EB015894, P41 EB027061, P30 NS076408, 1S10OD017974, UL1TR000114, and KL2TR000113).

A.S. received funding from the European Union's Horizon 2020 research and innovation program under the Marie Skłodowska-Curie grant agreement No 794986.

The content is solely the responsibility of the authors and does not necessarily represent the official views of the funding bodies.

Supplementary materials

Supplementary material associated with this article can be found, in the online version, at doi:10.1016/j.nicl.2020.102234.

References

Andersson, J.L.R., Skare, S., Ashburner, J., 2003. How to correct susceptibility distortions in spin-echo echo-planar images: application to diffusion tensor imaging. Neuroimage 20 (2), 870–888.

Andersson, J.L.R., Stamatios N, S., 2016. An integrated approach to correction for off-resonance effects and subject movement in diffusion MR imaging. Neuroimage 125, 1063–1078.

Barkhof, F., 2002. The clinico-radiological paradox in multiple sclerosis revisited. Curr. Opin. Neurol. 15 (3), 239–245.

Battaglini, M., Jenkinson, M., Stefano, Nde, 2012. Evaluating and reducing the impact of white matter lesions on brain volume measurements. Hum. Brain Mapp. 33 (9), 2062–2071.

Beer, A., Biberacher, V., Schmidt, P., Righart, R., Buck, D., Berthele, A., Kirschke, J., Zimmer, C., Hemmer, B., Mühlau, M., 2016. Tissue damage within normal appearing white matter in early multiple sclerosis: assessment by the ratio of T1-and T2-Weighted MR image intensity. J. Neurol. 263 (8), 1495–1502.

Burgetova, A., Seidl, Z., Krasensky, J., Horakova, D., Vaneckova, M., 2010. Multiple sclerosis and the accumulation of iron in the basal ganglia: quantitative assessment of brain iron using MRI T2 relaxometry. Eur. Neurol. 63 (3), 136–143.

Cercignani, M., Bozzali, M., Iannucci, G., Comi, G., Filippi, M., 2001. Magnetisation transfer ratio and mean diffusivity of normal appearing white and grey matter from patients with multiple sclerosis. J. Neurol. Neurosurg. Psychiatry 70 (3), 311–317.

Cercignani, M., Wheeler-Kingshott, C.G., 2019. From Micro- to Macro-Structures in multiple sclerosis: what is the added value of diffusion imaging. NMR Biomed. 32, e3888. https://doi.org/10.1002/nbm.3888.

Chen, X., Zhang, J., Kong, D., Chen, W., Zheng, J., 2018. Abnormal intrinsic functional hubs in Relapsing- Remitting Multiple sclerosis: evidence from a voxel-wise degree centrality analysis. Neuropsychiatry 8 (2), 448–459. https://doi.org/10.4172/Neuropsychiatry.1000366.

Cox, RW., 1996. AFNI: software for analysis and visualization of functional magnetic resonance neuroimages. Comput. Biomed. Res. 29 (3), 162–173.

Crespy, L., Zaaraoui, W., Lemaire, M., Rico, A., Faivre, A., Reuter, F., Malikova, I., Confort-Gouny, S., Cozzone, P.J., Pelletier, J., 2011. Prevalence of grey matter pathology in early multiple sclerosis assessed by magnetization transfer ratio imaging. PLoS One 6 (9), e24969.

Dortch, RD., Harkins, KD., Juttukonda, MR., Gore, JC., Does, MD., 2013. Characterizing inter-compartmental water exchange in myelinated tissue using relaxation exchange spectroscopy. Magn. Reson. Med. 70 (5), 1450–1459.

Faivre, A., Robinet, E., Guye, M., Rousseau, C., Maarouf, A., Troter, Ale, Zaaraoui, W., et al., 2016. Depletion of brain functional connectivity enhancement leads to disability progression in multiple sclerosis: a longitudinal resting-state FMRI study. Multiple Sclerosis J. 22 (13), 1695–1708. https://doi.org/10.1177/1352458516628657.

Filippi, M., Rocca, M.A., Martino, G., Horsfield, M.A., Comi, G., 1998. Magnetization transfer changes in the normal appearing white matter precede the appearance of enhancing lesions in patients with multiple sclerosis. Ann. Neurol. 43 (6), 809–814. https://doi.org/10.1002/ana.410430616.

Filippi, M., Rocca, MA., Ciccarelli, O., Stefano, Nde, Evangelou, N., Kappos, L., Rovira, A., Sastre-Garriga, J., Tintorè, M., Frederiksen, JL., 2016. MRI criteria for the diagnosis of multiple sclerosis: magnims consensus guidelines. Lancet Neurol. 15 (3), 292–303.

Garwood, M., DelaBarre, L., 2001. The return of the frequency sweep: designing adiabatic pulses for contemporary nmr. J. Magn. Reson. 153 (2), 155–177.

Giannetti, P., Politis, M., Su, P., Turkheimer, F.E., Malik, O., Keihaninejad, S., Wu, K., Waldman, A., Reynolds, R., Nicholas, R., 2014. Increased PK11195-PET binding in normal-appearing white matter in clinically isolated syndrome. Brain 138 (1), 110–119.

Glasser, MF., Sotiropoulos, SN., Anthony Wilson, J., Coalson, TS., Fischl, B., Andersson, JL., Xu, J., Jbabdi, S., Webster, M., Polimeni, JR., 2013. The minimal preprocessing pipelines for the human connectome project. Neuroimage 80, 105–124.

Glasser, MF., Essen, DC.V, 2011. Mapping human cortical areas in vivo based on myelin content as revealed by T1- and T2-Weighted MRI. J. Neurosci. 31 (32), 11597–11616. https://doi.org/10.1523/JNEUROSCI.2180-11.2011.

Gracien, R.-M., Reitz, SC., Hof, S.M., Fleischer, V., Zimmermann, H., Droby, A., Steinmetz, H., Zipp, F., Deichmann, R., Klein, JC., 2016. Changes and variability of proton density and T1 relaxation times in early multiple sclerosis: MRI markers of neuronal damage in the cerebral cortex. Eur. Radiol. 26 (8), 2578–2586.

Green, AJ., Gelfand, JM., Cree, BA., Bevan, C., John Boscardin, W., Mei, F., Inman, J., Arnow, S., Devereux, M., Abounasr, A., 2017. Clemastine fumarate as a remyelinating therapy for multiple sclerosis (ReBUILD): a randomised, controlled, double-blind, crossover trial. Lancet 390 (10111), 2481–2489.

Hakkarainen, H., Sierra, A., Mangia, S., Garwood, M., Michaeli, S., Gröhn, O., Liimatainen, T., 2016. MRI relaxation in the presence of fictitious fields correlates with myelin content in normal rat brain. Magn. Reson. Med. 75 (1), 161–168.

Jenkinson, M., Bannister, P., Brady, M., Smith, S., 2002. Improved optimization for the robust and accurate linear registration and motion correction of brain images. Neuroimage 17 (2), 825–841.

Jenkinson, M., Beckmann, CF., Behrens, T.E.J., Woolrich, MW., Smith, SM., 2012. Fsl. Neuroimage 62 (2), 782–790.

Kutzelnigg, A., Lucchinetti, CF., Stadelmann, C., Brück, W., Rauschka, H., Bergmann, M., Schmidbauer, M., Parisi, JE., Lassmann, H., 2005. Cortical demyelination and diffuse white matter injury in multiple sclerosis. Brain 128 (11), 2705–2712. https://doi.org/10.1093/brain/awh641.

Langkammer, C., Krebs, N., Goessler, W., Scheurer, E., Ebner, F., Yen, K., Fazekas, F., Ropele, S., 2010. Quantitative MR imaging of brain iron: a postmortem validation study. Radiology 257 (2), 455–462.

Levitt, MH., Freeman, R., Frenkiel, T., 1982. Broadband heteronuclear decoupling. J. Magn. Reson. 47 (2), 328–330 1969.

Liimatainen, T., Laakso, H., Idiyatullin, D., Mangia, S., Michaeli, S., 2018. Capturing exchange using periodic radiofrequency irradiation. J. Magn. Reson. 296

(November), 79–84. https://doi.org/10.1016/j.jmr.2018.09.001.
Liimatainen, T., Sierra, A., Hanson, T., Sorce, D.J., Ylä-Herttuala, S., Garwood, M., Michaeli, S., Gröhn, O., 2012. Glioma cell density in a rat gene therapy model gauged by water relaxation rate along a fictitious magnetic field. Magn. Reson. Med. 67 (1), 269–277.
Liimatainen, T., Sorce, DJ., O'Connell, R., Garwood, M., Michaeli, S., 2010. MRI contrast from relaxation along a fictitious field (RAFF). Magn. Reson. Med. 64 (4), 983–994.
Lukes, S.A., Crooks, L.E., Aminoff, M.J., Kaufman, L., Panitch, H.S., Mills, C., Norman, D., 1983. Nuclear magnetic resonance imaging in multiple sclerosis. Ann. Neurol. 13 (6), 592–601. https://doi.org/10.1002/ana.410130603.
Mangia, S., Carpenter, AF., Tyan, AE., Eberly, LE., Garwood, M., Michaeli, S., 2014. Magnetization transfer and adiabatic T1ρ MRI reveal abnormalities in normal-appearing white matter of subjects with multiple sclerosis. Multiple Scler. J. 20 (8), 1066–1073.
Mangia, S., Liimatainen, T., Garwood, M., Michaeli, S., 2009. Rotating frame relaxation during adiabatic pulses vs. conventional spin lock: simulations and experimental results at 4 T. Magn. Reson. Imaging 27 (8), 1074–1087.
Mangia, S., Svatkova, A., Mascali, D., Nissi, M.J., Burton, P.C., Bednarik, P., Auerbach, E.J., Giove, F., Eberly, L.E., Howell, M.J., 2017. Multi-Modal brain MRI in subjects with PD and IRBD. Front. Neurosci. 11, 709. https://doi.org/10.3389/fnins.2017.00709.
McCreary, CR., Bjarnason, TA., Skihar, V., Ross Mitchell, J., Wee Yong, V., Dunn, JF., 2009. Multiexponential T2 and magnetization transfer mri of demyelination and remyelination in murine spinal cord. Neuroimage 45 (4), 1173–1182.
Michaeli, S., Burns, TC., Kudishevich, E., Harel, N., Hanson, T., Sorce, DJ., Garwood, M., Low, WC., 2009. Detection of neuronal loss using T1ρ MRI assessment of 1H2O spin dynamics in the aphakia mouse. J. Neurosci. Methods 177 (1), 160–167.
Michaeli, S., Oez, G., Sorce, D.J., Garwood, M., Ugurbil, K., Majestic, S., Tuite, P., 2007. Assessment of brain iron and neuronal integrity in patients with parkinson's disease using novel MRI contrasts. Mov. Disord. 22 (3), 334–340.
Michaeli, S., Sorce, DJ., Idiyatullin, D., Ugurbil, K., Garwood, M., 2004. Transverse relaxation in the rotating frame induced by chemical exchange. J. Magn. Reson. 169 (2), 293–299.
Michaeli, S., Sorce, DJ., Jr, CS.S, Ugurbil, K., Garwood, M., 2006. T1ρ MRI contrast in the human brain: modulation of the longitudinal rotating frame relaxation shutter-speed during an adiabatic RF pulse. J. Magn. Reson. 181 (1), 135–147.
Mitsumori, F., Watanabe, H., Takaya, N., 2009. Estimation of brain iron concentration in vivo using a linear relationship between regional iron and apparent transverse relaxation rate of the tissue water at 4.7 t. Magn. Res. Med. 62 (5), 1326–1330.
Moll, NM., Rietsch, AM., Thomas, S., Ransohoff, AJ., Lee, J.-.C., Fox, R., Chang, A., Ransohoff, RM., Fisher, E., 2011. Multiple sclerosis normal-appearing white matter: pathology – Imaging correlations. Ann. Neurol. 70 (5), 764–773.
Mottershead, J.P., Schmierer, K., Clemence, M., Thornton, J.S., Scaravilli, F., Barker, G.J., Tofts, P.S., Newcombe, J., Cuzner, M.L., Ordidge, R.J., 2003. High field MRI correlates of myelin content and axonal density in multiple sclerosis. J. Neurol. 250 (11), 1293–1301.
Nestrasil, I., Michaeli, S., Liimatainen, T., Rydeen, C.E., Kotz, C.M., Nixon, J.P., Hanson, T., Tuite, PJ., 2010. T 1ρ and T 2ρ MRI in the evaluation of Parkinson's disease. J. Neurol. 257 (6), 964–968.
Polman, CH., Reingold, SC., Banwell, B., Clanet, M., Cohen, JA., Filippi, M., Fujihara, K., Havrdova, E., Hutchinson, M., Kappos, L., 2011. Diagnostic criteria for multiple sclerosis: 2010 revisions to the mcdonald criteria. Ann. Neurol. 69 (2), 292–302.
Rae-Grant, A., Day, GS., Marrie, R.A., Rabinstein, A., AC Cree, B., Gronseth, GS., Haboubi, M., Halper, J., Hosey, JP., Jones, DE., 2018. Practice guideline recommendations summary: disease-Modifying therapies for adults with multiple sclerosis: report of the guideline development, dissemination, and implementation subcommittee of the american academy of neurology. Neurology 90 (17), 777–788.
Reuter, M., Diana Rosas, H., Fischl, B., 2010. Highly accurate inverse consistent registration: a robust approach. Neuroimage 53 (4), 1181–1196.
Rocca, MA., Valsasina, P., Meani, A., Falini, A., Comi, G., Filippi, M., 2016. Impaired functional integration in multiple sclerosis: a graph theory study. Brain Struct. Funct. 221 (1), 115–131. https://doi.org/10.1007/s00429-014-0896-4.
Ropele, S., Fazekas, F., 2009. Magnetization transfer MR imaging in multiple sclerosis. Neuroimaging Clin. 19 (1), 27–36.
Salimi-Khorshidi, G., Douaud, G., Beckmann, C.F., Glasser, MF., Griffanti, L., Smith, SM., 2014. "Automatic denoising of functional MRI data: combining independent component analysis and hierarchical fusion of classifiers." Neuroimage 90, 449–468.
Sarchielli, P., Presciutti, O., Tarducci, R., Gobbi, G., Alberti, A., Pelliccioli, G.P., Chiarini, P., Gallai, V., 2002. Localized 1 h magnetic resonance spectroscopy in mainly cortical gray matter of patients with multiple sclerosis. J. Neurol. 249 (7), 902–910.
Satzer, D., DiBartolomeo, C., Ritchie, M.M., Storino, C., Liimatainen, T., Hakkarainen, H., Idiyatullin, D., Mangia, S., Michaeli, S., Parr, AM., 2015. Assessment of dysmyelination with RAFFn MRI: application to murine MPS I. PLoS One 10 (2), e0116788.
Schmierer, K., Scaravilli, F., Altmann, D.R., Barker, GJ., Miller, DH., 2004. Magnetization transfer ratio and myelin in postmortem multiple sclerosis brain. Ann. Neurol. 56 (3), 407–415.
Schmithorst, VJ., Wilke, M., Dardzinski, BJ., Holland, SK., 2002. Correlation of white matter diffusivity and anisotropy with age during childhood and adolescence: a cross-sectional diffusion-tensor mr imaging study. Radiology 222 (1), 212–218.
Sierra, A., Michaeli, S., Niskanen, J.-.P., Valonen, P.K., Gröhn, H.I., Ylä-Herttuala, S., Garwood, M., Gröhn, OH., 2008. Water spin dynamics during apoptotic cell death in glioma gene therapy probed by T1ρ and T2ρ Magn. Reson. Med. 59 (6), 1311–1319.
Silver, M.S., Joseph, R.I., H.oult, D.I., 1984. Highly selective Π2 and π pulse generation. J. Magn. Reson. 59 (2), 347–351. https://doi.org/10.1016/0022-2364(84)90181-1. (1969).
Smith, SM., Beckmann, CF., Andersson, J., Auerbach, EJ., Bijsterbosch, J., Douaud, G., Duff, E., Feinberg, DA., Griffanti, L., Harms, MP., 2013. Resting-State FMRI in the human connectome project. Neuroimage 80, 144–168.
Stephenson, E., Nathoo, N., Mahjoub, Y., Dunn, J.F., Wee Yong, V., 2014. Iron in multiple sclerosis: roles in neurodegeneration and repair. Nat. Rev. Neurol. 10 (8), 459.
Tartaglia, M.C., Narayanan, S., De Stefano, N., Arnaoutelis, R., Antel, S.B., Francis, S.J., Santos, A.C., Lapierre, Y., Arnold, D.L., 2002. Choline is increased in pre-lesional normal appearing white matter in multiple sclerosis. J. Neurol. 249 (10), 1382–1390. https://doi.org/10.1007/s00415-002-0846-6.
Torkildsen, Ø., Myhr, K.-M., Bø, L., 2016. Disease-Modifying treatments for multiple sclerosis – a review of approved medications. Eur. J. Neurol. 23 (S1), 18–27.
Traboulsee, A., Dehmeshki, J., Peters, KR., Griffin, C.M., Brex, P.A., Silver, N., Ciccarrelli, O., Chard, D.T., Barker, G.J., Thompson, A.J., 2003. Disability in multiple sclerosis is related to normal appearing brain tissue MTR histogram abnormalities. Multiple Scler. J. 9 (6), 566–573.
Uddin, MdN, Figley, T.D., Ann Marrie, R., Figley, CR., 2018. "Can T1w/T2w ratio be used as a myelin-specific measure in subcortical structures? Comparisons between FSE-Based T1w/T2w ratios, GRASE-Based T1w/T2w ratios and multi-echo GRASE-Based myelin water fractions." NMR Biomed. 31 (3), e3868. https://doi.org/10.1002/nbm.3868.
Wattjes, MP., Rovira, À., Miller, D., Yousry, TA., Sormani, MP., Stefano, Nde, Tintoré, M., Auger, C., Tur, C., Filippi, M., 2015. Evidence-based guidelines: magnims consensus guidelines on the use of MRI in multiple sclerosis—establishing disease prognosis and monitoring patients. Nat. Rev. Neurol. 11 (10), 597.
Werring, D.J., Brassat, D., Droogan, A.G., Clark, C.A., Symms, M.R., Barker, G.J., MacManus, D.G., Thompson, A.J., Miller, D.H., 2000. The pathogenesis of lesions and normal-appearing white matter changes in multiple sclerosis: a serial diffusion MRI study. Brain 123 (Pt 8), 1667–1676.
Wiggermann, V., Torres, E.H., Vavasour, I.M., Wayne Moore, G.R., Laule, C., MacKay, AL., B. Li, DK., Traboulsee, A., Rauscher, A., 2013. Magnetic resonance frequency shifts during acute ms lesion formation. Neurology 81 (3), 211–218. https://doi.org/10.1212/WNL.0b013e31829bfd63.
Wuerfel, J., Bellmann-Strobl, J., Brunecker, P., Aktas, O., McFarland, H., Villringer, A., Zipp, F., 2004. Changes in cerebral perfusion precede plaque formation in multiple sclerosis: a longitudinal perfusion MRI study. Brain: A Journal of Neurology 127 (Pt 1), 111–119. https://doi.org/10.1093/brain/awh007.
Yarnykh, VL., 2012. Fast macromolecular proton fraction mapping from a single off-resonance magnetization transfer measurement. Magn. Reson. Med. 68 (1), 166–178.
Yarnykh, VL., Bowen, JD., Samsonov, A., Repovic, P., Mayadev, A., Qian, P., Gangadharan, B., Keogh, BP., Maravilla, KR., Henson, LK.J, 2014. Fast whole-brain three-dimensional macromolecular proton fraction mapping in multiple sclerosis. Radiology 274 (1), 210–220.
Young, I.R., Hall, A.S., Pallis, C.A., Legg, N.J., Bydder, G.M., Steiner, R.E., 1981. Nuclear magnetic resonance imaging of the brain in multiple sclerosis. Lancet 2 (8255), 1063–1066.